8-2019

Exploring the Role of Evaporation and Precipitation Rates on Mangrove Island Morphology

Isamar M. Cortés
Montclair State University

Abstract

Mangroves are salt tolerant species of trees that grow in tropical and subtropical environments. Mangroves provide ecosystem services to societies along marine environments, including storm protection, coastal biodiversity, and blue carbon storage. However, as the importance of mangrove ecosystems has become clearer over recent years, their coverage has been reduced through mismanagement and climate impacts. For instance, in terms of climate warming, mangroves cannot survive under abnormally high rates of net evaporation when soil stressor concentrations (e.g., sulfate, sulfide) increase above threshold conditions. To study the effects of this climate driver phenomenon on mangrove islands, we are examining mangrove islands, which typically grow on carbonate platforms, isolated from human activities. In high net evaporation zones (where evaporation is greater than precipitation) such as Florida, Bahamas or Puerto Rico, the soil moisture potential is altered by high net evaporation, which affects mangrove islands by undergoing species zonation and die off within the interior. In contrast, mangrove islands within a low or negative net evaporation zone (relative to precipitation), such as Belize, are typically large and grow to the maximum extent allowed by the carbonate platform. We quantified this phenomenon with a simple mathematical model that relates island vegetated area with the rate of net evaporation, the hydraulic conductivity of the soil, and the salinity threshold for mangrove growth (used as a proxy for soil stressor concentration). We estimated net evaporation rates in the Caribbean using existing meteorological data for the last ~20 years, and the hydraulic conductivity as a function of the area of red mangroves versus black mangroves, which requires remote sensing analysis. Areas with a greater proportion of red mangroves can tend to have higher hydraulic conductivity while those with a greater proportion of black mangroves tend to have lower hydraulic conductivity. Preliminary model results coupled with data from a number of mangrove islands in the Caribbean support the initial premise that an increase in net evaporation reduces mangrove vegetated area. Future work will focus on expanding the mangrove island database and better constrain the input parameter values with local observations.

MONTCLAIR STATE UNIVERSITY

Exploring the role of evaporation and precipitation on mangrove island morphology

By: Isamar M. Cortés

A Master's Thesis Submitted to the Faculty of

Montclair State University

In Partial Fulfillment of the Requirements

For the Degree of

Master of Science

August 2019

College of Science and Mathematics

Department of Earth and Environmental Science

Thesis Committee:

[redacted]

Dr. Jorge Lorenzo- Trueba
Thesis Sponsor

[redacted]

Dr. Mark Chopping
Committee Member

[redacted]

Dr. Greg Pope
Committee Member

Exploring the Role of Evaporation and Precipitation Rates on Mangrove Island Morphology

A Thesis

Submitted in partial fulfillment of the requirements

For the degree of Master of Science

By

Isamar Cortes

Department of Earth and Environmental Science; Montclair State University

Montclair State University

Montclair, NJ

2019

Table of Contents

1. Introduction

Mangroves are a tropical and subtropical species of tree that exist in coastal marine environments. Across the globe, there are 54 species of mangroves (Parida et al. 2002) that exist in over 100 countries. They flourish in tropical settings between 25° north and south of the equator. At the interface between aquatic and terrestrial ecosystems, mangroves act as the first line of defense for coastal communities (Parida et al. 2012, Barbier 2016, Cintron et al. 1978). Mangroves are one of the most productive marine ecosystems, covering thousands of square kilometers of tropical and subtropical coastlines (Chen & Twilley 1998, Twilley et al. 1992), along with providing numerous ecosystem services. For instance, mangroves are productive nurseries for thousands of aquatic species, including crabs, sharks and macro benthic organisms. Mangroves also provide storm protection as they buffer winds and dampen wave energy during storm events (Barbier 2016). Additionally, mangroves provide blue carbon storage (Phang et al. 2015). Despite their importance, however, mangrove ecosystems have declined by over 30% during the past few decades (Barbier 2016). Such reduction is due to human development (Berger et al. 2008), as well as climatic factors (Alongi 2008) that affect the concentration of stressors such as sulfate, sulfide and salinity (Twilley et al. 1992). The analysis of this work specifically focused on mangrove islands (figure 1), which are low-lying topographic relief islands predominantly filled with mangrove ecosystems (Lugo et al. 1974). These islands are defined as stand alone overwash forests within their respective carbonate platforms. These areas do not have direct anthropogenic stressors, which can otherwise result in mangrove degradation. Additionally, this study focuses on the Caribbean, an ideal location for this work as it lies in a positive net evaporation (i.e. evaporation – precipitation) zone in the most part, with the exception of Belize islands.

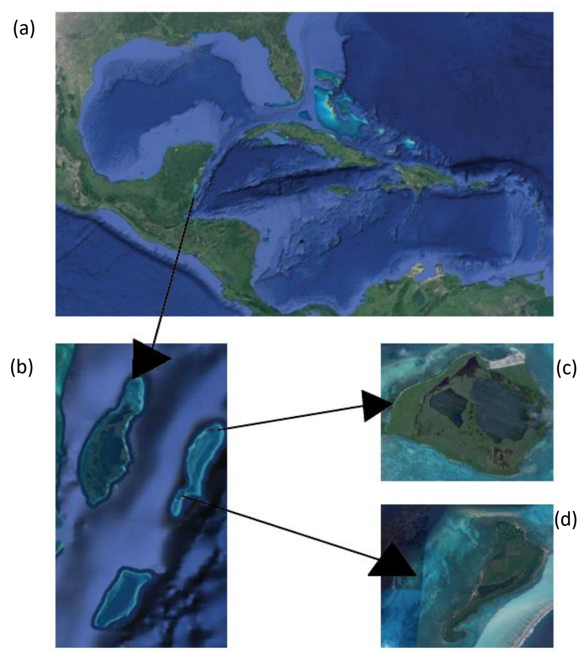

Figure 1 shows examples of mangrove islands (c, d) established on a carbonate platform in Belize (b) within the Caribbean (a) The arrows indicate the corresponding locations.

Changes in evaporation and precipitation rates can affect soil stressor concentrations such as sulfate, sulfide and salinity (Krauss et al. 2006, Lugo 1980). In turn, soil stressor concentration can regulate survival, height and zonation of mangrove ecosystems (Twilley & Chen 1998). Mangroves have evolved the ability to survive in saline environments due to their root systems. Their roots are able to filter out salinity from ocean water in order to acquire freshwater. However, although mangroves can tolerate saline environments, there is a threshold salt concentration beyond which they cannot survive (Cintron et al. 1978, Ball et al. 1988, Twilley et al. 1992, Lovelock et al. 2016). In particular, as depicted by Figure 1, when salt concentration is higher than this critical value (i.e., $S>=Sc$), the rate of degradation of organic matter through respiration exceeds the rate of mangrove biomass productivity (Twilley et al. 1992). The value of the critical salinity concentration threshold (i.e., Sc) depends on the mangrove type. The Caribbean has three dominant mangrove species: *Rhizophora mangle* (red), *Avicennia germans* (black) and *Laguncularia Racemosa* (white) mangroves predominantly (Lugo 1980). Black and white mangroves are able to handle higher salinity concentrations than red mangroves. It is vital to note that while white mangroves are part of the species of mangroves existing along the Caribbean, they prefer areas with elevation where they can compete against black and red mangroves. For the purpose of this research, when dictating critical salinity concentration thresholds, we study red and black mangroves as they predominantly exist in low-lying overwash mangrove islands. While red mangroves can tolerate a soil salinity of ~70 ppt, the black mangrove is able to tolerate salinity at ~100 ppt (Twilley & Chen 1998). Soil stressors (i.e. sulfate, sulfide, salinity) dictate mangrove species zonation, which is critical to understanding the morphology. At a certain salinity concentration, mangrove ecosystems will undergo degradation. After this point, respiration outcompetes mangrove production until mangroves cannot continue to grow in total mass. Production and respiration in these ecosystems both decrease to create die off within the interior.

We hypothesize that as net evaporation increases, mangrove vegetated area decreases. To test this hypothesis, we use the Caribbean as our study site as there is a range in net evaporation rates. Using an area with a range in net evaporation values allows us to study differences in areas with high versus low net evaporation zones. Net evaporation affects the fresh water balance within an ecosystem by either increasing or decreasing the fresh water availability within the island. Positive net evaporation (i.e. evaporation greater than precipitation) decreases the freshwater within the system, while negative net evaporation (i.e. precipitation greater than evaporation) increases the freshwater content within an ecosystem. Depending on the net evaporation, the salinity concentration will either increase or decrease. In a positive net evaporation zone, the salinity concentration increases within an island as the freshwater decreases within the system (Figure 2). A negative net evaporation area adds freshwater into the system in the form of precipitation, thus, decreasing the salinity concentration within the island, allowing mangroves to grow to the extent of their carbonate platform (Figure 2b).

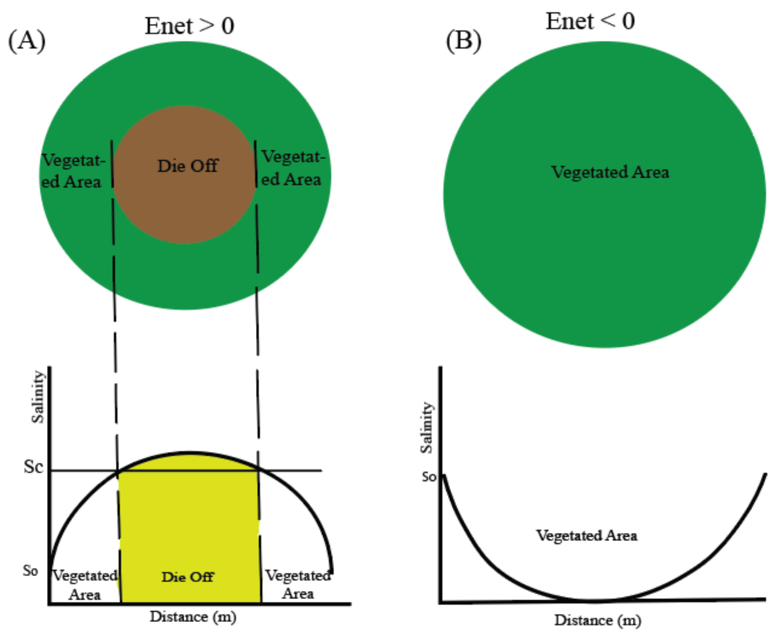

Figure 2a. The salt concentration profile for an island under a positive net evaporation rate. Salinity increases towards the center of the island, reaching values beyond mangrove survival (i.e.,critical salinity, Sc). In contrast, Figure 2b depicts a mangrove island in a negative net evaporation zone in which salinity decreases towards the interior of the island.

2. <u>Methods</u>

In order to test the hypothesis, we first use NASA satellite imagery and WHOI OAFLUX imagery to estimate the average net evaporation rates for mangrove islands in the Caribbean. Second, we use Digital Globe Inc. imagery through Google Earth Pro to estimate mangrove vegetated for each individual island in our region of study. We then verify that these are in fact mangrove islands through global mangrove watch. Third, we develop a numerical model that relates mangrove vegetated area and net evaporation rates.

<u>2.1 Net Evaporation Map</u>

We used precipitation and evaporation datasets to build an average net evaporation map for the Caribbean. First, we estimate precipitation rates using the Tropical Rain Measuring Mission (TRMM), which was launched by NASA and the Japan Aerospace Exploration Agency (JAXA) in 1997. This dataset provides precipitation data for areas 40° North and South of the equator from 1997 to present, and with a 0.25° x 0.25° resolution. We use this dataset to estimate precipitation rate values for our study sites (Figure 5). For additional details, check the section “Methods for TRMM data extraction” in the Appendix. Second, we collected evaporation data using the Wood Hole Oceanographic Institution (WHOI) Multidecade flux datasets. The multidecade flux datasets contain evaporation rates from 1958 to Present, with 1° x 1° spatial resolution. We used these data to estimate evaporation rates in our study sites (Figure 5). For additional details, check the section “Methods to extract evaporation rates" in the Appendix. Third, we combined Figures 3(a) and 3(b) to create a net evaporation map as depicted in Figure 3 (c), where net evaporation is described as the difference between evaporation and precipitation rates. Using this map, we were able to determine average net evaporation rates in specific locations within the Caribbean.

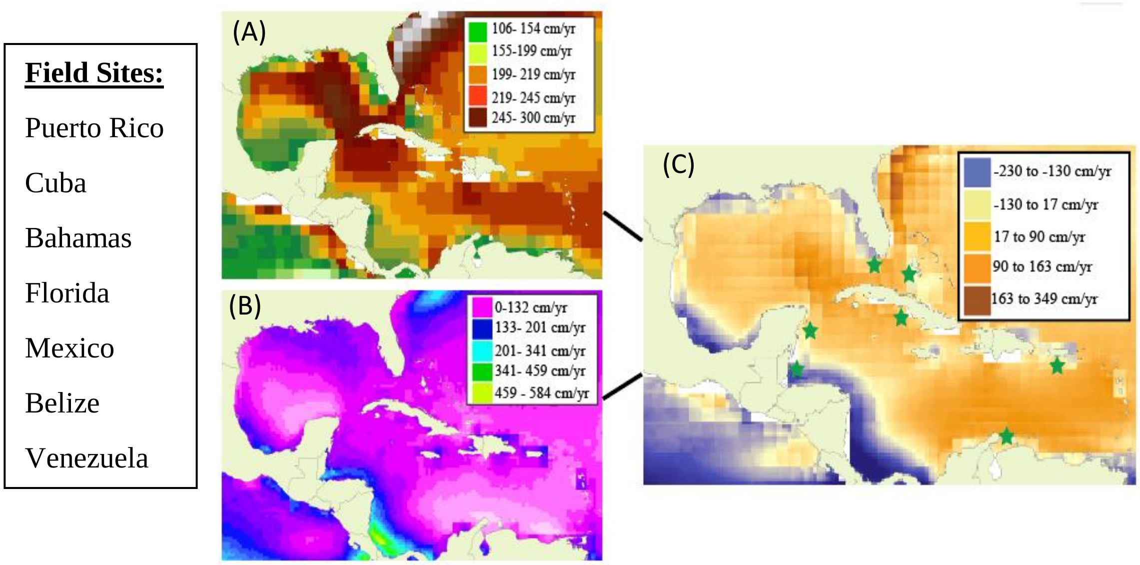

Figure 3. (a) An evaporation map based on yearly data (b) an average precipitation map derived from NASA TRMM datasets. (c) a net evaporation map that shows positive net evaporation across the Caribbean.

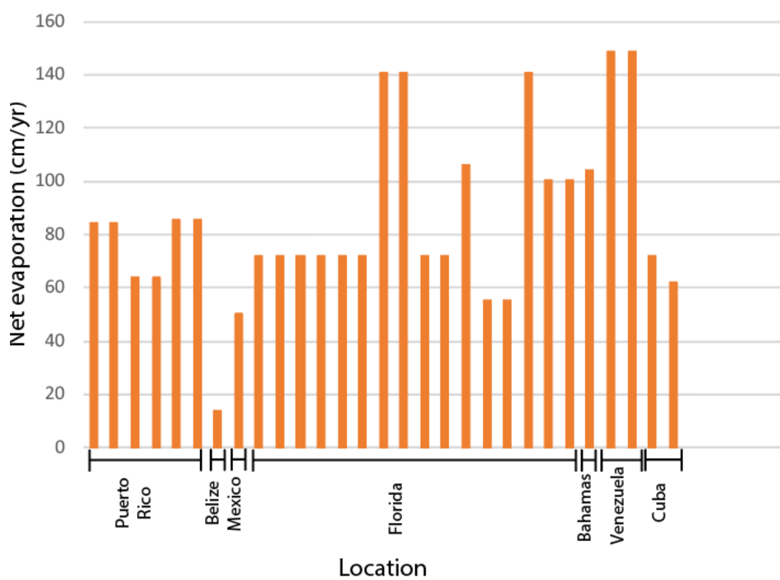

Figure 4. Net evaporation rates based on areas across the Caribbean. We can already begin to speculate that islands in Florida will have less vegetation than islands in Belize.

2.2 Mangrove island database

We built a database of mangrove islands, extracting island information with Google Earth Pro (GEP) and verifying that it is in fact a mangrove island using Global Mangrove Watch (citation), which allows us to eliminate islands that are not predominantly mangrove ecosystems (Thomas 2017). Mangrove islands are located in areas of both high net evaporation rates, where evaporation is greater than precipitation, as well as low or negative net evaporation rates (Figures 4, 5). Direct anthropogenic effects on these islands are very limited as they are generally located in remote areas around the Caribbean. Additionally, all the islands in our database are low-lying and therefore we can neglect the effect of elevation changes on mangrove zonation.

As we might expect, mangrove islands in high net evaporation zones such as Florida, Bahamas or Puerto Rico often present die-off within the interior (Figure 5). In contrast, mangrove islands within a low or negative net evaporation zone such as Belize, are typically large and grow to the maximum extent allowed by the carbonate platform (Figure 5).

Figure 5 shows Google Earth imagery from different mangrove islands in contrasting net evaporation zones. The islands shown in the top two panels are in a negative net evaporation zone while the rest are in a positive net evaporation zone.

2.3 Modeling framework: Relationship between vegetated area and net evaporation rates

In this section, we develop a theoretical framework to quantify the relationship between mangrove vegetated area and the net evaporation rate *Enet*, which in turn controls the concentration of soil stressors within the island (Figure 2). We define the balance in soil stressor *S* at any location in the island as follows:

$$\frac{dS}{dt} = \frac{dq}{dx} + \gamma \qquad (1)$$

where q is the flux of soil stressor at any location *x* within the island, and $\gamma = Enet \cdot b$, where *b* is a conversion factor described as the ratio between a reference salinity and a reference soil depth within which the stressor is transported. For simplicity, we assume a linear relationship between the flux and the gradient in soil stressor as follows:

$$q = k\frac{dS}{dx} \qquad (2)$$

where *k* is the hydraulic conductivity in meters per year. Combining (1) and (2), we obtain the so-called linear diffusion equation with a source term for the net evaporation rate:

$$\frac{ds}{dt} = k\frac{d^2S}{dx^2} + \gamma \qquad (3)$$

In order to solve equation (3), we need two boundary conditions. The first boundary condition matches the concentration in soil stressor at the edge of the island to the stressor concentration in the ocean.

$$S(x = R) = So \qquad (4)$$

The second boundary condition relies on the island being symmetric, which results in a maximum or a minimum in stressor concentration at x=0, i.e.,

$$\frac{dS}{dx}(x = 0) = 0 \qquad (5)$$

In this way, we can integrate equation (3) twice and arrive to the following quadratic equation:

$$S = -\alpha x^2 + So + \alpha R^2 \qquad (6)$$

This quadratic formula describes the stressor concentration as a function of α is defined as $\alpha = \gamma/2 \cdot k$

The model also assumes a critical salt concentration *Sc* beyond which black mangrove ecosystems cannot survive and a die-off region forms. This is justified by the fact that black mangroves are the most salt-tolerant among mangrove species in the Caribbean (Twilley & Chen 1992).

Assuming a circular shape for the islands combined with the salt concentration profile described by equation (2), we can express the vegetated area within the island *Av* as follows:

$$Av = \frac{\pi(Sc - So)}{\alpha} \quad (5)$$

As described by equation (5), not only net evaporation rate is an important factor determining mangrove vegetated are, but also hydraulic conductivity (Figure 6, 7 and 8). In particular, as hydraulic conductivity increases, mangrove vegetation also increases. Islands where the hydraulic conductivity is low, experience higher soil stressor concentrations. Higher hydraulic conductivity rates allow for flushing to occur, thus, decreasing soil stressor concentrations (Figure 6). Additionally, ocean salinity also play a significant role on the development of mangrove vegetation. As ocean salinity increases, the gap between ocean salinity concentration and the critical salinity concentration shortens. It then becomes simpler to reach the critical salinity concentration threshold in high net evaporation zones (Figure 6).

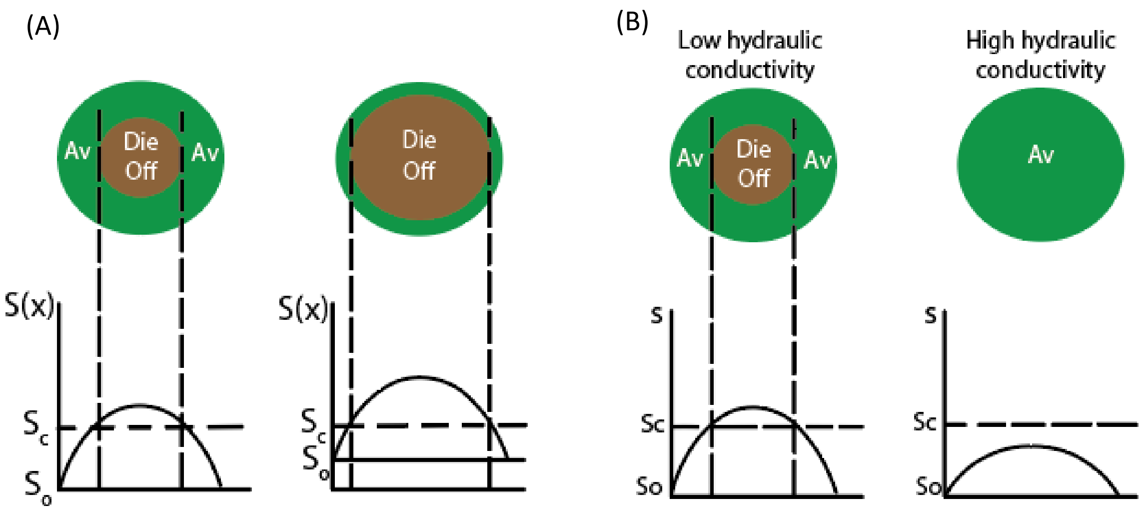

Figure 6. How ocean salinity and hydraulic conductivity affect the vegetated area.

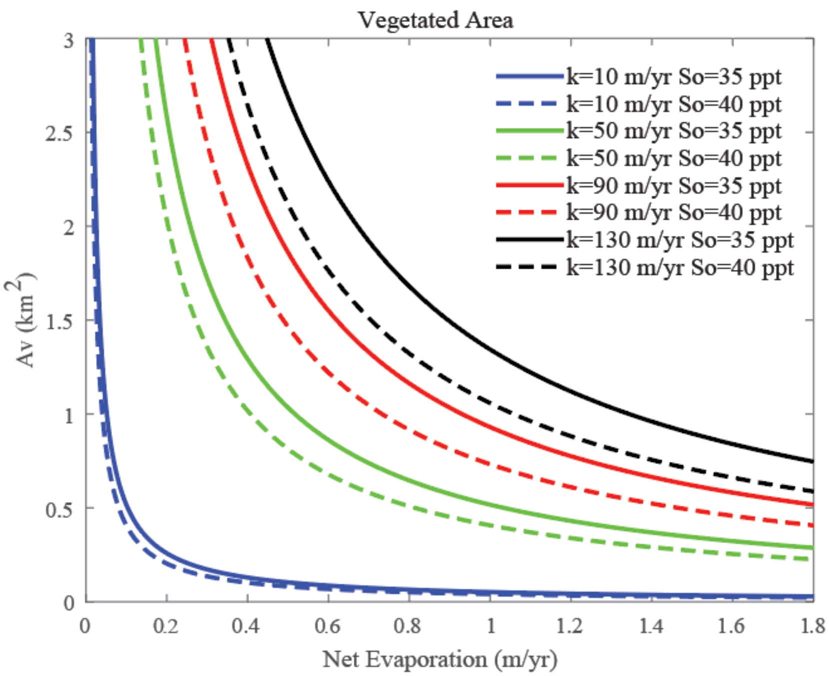

Figure 7. The decrease in vegetated area as a function of net evaporation, hydraulic conductivity *k* and ocean salinity *So*.

Figures 7 illustrates the relationship between vegetated area, net evaporation rates, hydraulic conductivity, and ocean salinity. As net evaporation rate increases, or hydraulic conductivity decreases, vegetated area diminishes. The range of hydraulic conductivity values (10-130 m/yr) falls within the range of values typically observed in peaty soils. Additionally, the range of values considered for ocean salinity (35-40 ppt) also fall within the range typically observed in the Caribbean (Lagerloef et al. 2008, Schmidt et al. 2004). As we might expect, the net evaporation rate plays a major role in determining the vegetated area of mangrove islands. Mangrove vegetated area is also very sensitive to changes in hydraulic conductivity, especially when both hydraulic conductivity and net evaporation rates are low. In contrast, the effect of ocean salinity on vegetated area is of second order when hydraulic conductivity is low, but gains weight as hydraulic conductivity increases.

Figure 8 depicts vegetated area in terms of the net evaporation rate and hydraulic conductivity values. Both Figures 7 and 8 suggest that the highest mangrove vegetated area tends to occur when the net evaporation rate is highest and the hydraulic conductivity is lowest. The results of tests of this theoretical result against observations are presented in the last section of the manuscript.

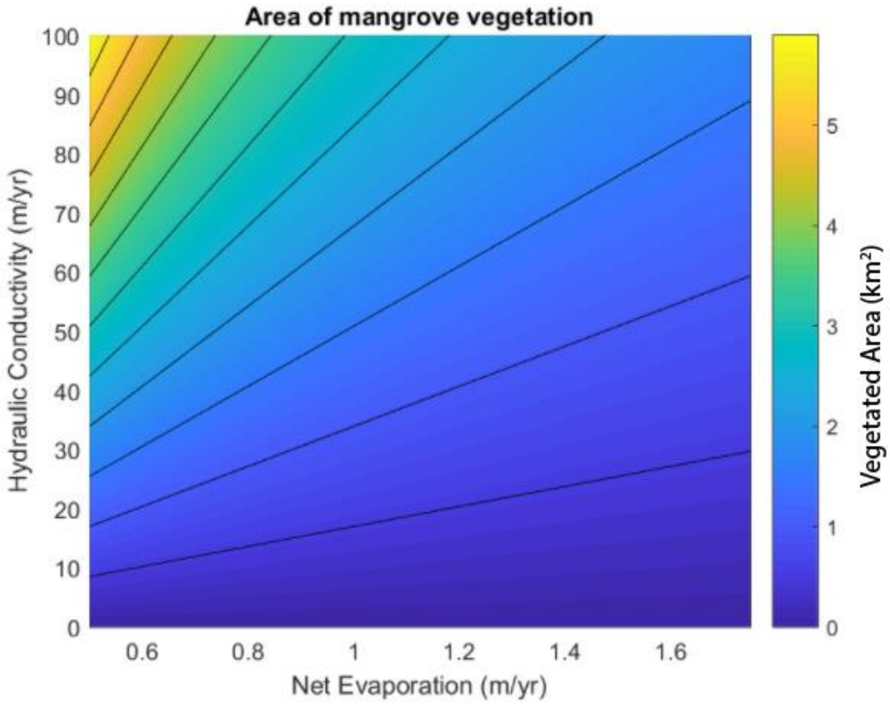

Figure 8. How mangrove vegetated area is affected by net evaporation and hydraulic conductivity. As net evaporation increase and hydraulic conductivity decreases, mangrove vegetated area decreases.

2.4. Estimating Hydraulic Conductivity

We estimate the hydraulic conductivity of the soil using the area of red mangroves in each island. As we decrease hydraulic conductivity, salt tends to accumulate in the soil instead of flushing out of the system, which results in a steeper increase in salt concentration towards the center of the island (Figure 5a). The steeper the salt concentration profile, the faster the succession of mangrove species from red to black, and die off in the interior (Twilley & Chen 1992, Cintron et al. 1978). Red mangrove critical salinity concentration is Sc_R~72 ppt (Cintron et al. 1978), whereas the value for black mangroves is Sc_B~ 100 ppt (Cintron et al. 1978). In contrast, the gradient of the salt concentration profile in an island with a high hydraulic conductivity is milder, resulting in a larger area

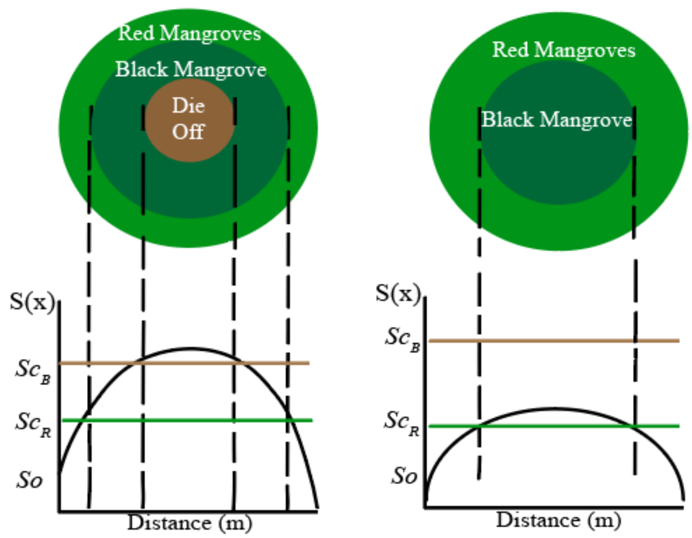

Figure 9. The effect of a low (a) and a high (b) hydraulic conductivity on mangrove island zonation.

of red mangroves (Figure 5b). We do not include white mangroves in this representation as they only appear in sparse areas with higher elevation.

In order to arrive to an expression for the hydraulic conductivity k, we combine the quadratic profile in equation (4) with the critical salt concentration of red mangroves. After some algebra, we arrive to the following equation:

$$k = \frac{\gamma \cdot Ar}{2(Sc_R - So)\pi} \tag{6}$$

where Ar is the area of red mangroves, Sc_R is the critical salinity concentration of red mangroves.

In order to estimate the area of red and black mangroves in each island using near infrared false color composite imagery (Figure 9). In particular, we use their surface reflectance values to create spectral plot, distinguishing the reflectance variance between red and black mangroves (see Figure 10). False color composites allow for specific distinction in areas of interest. For example, the most widely tested false color composite to use when studying vegetation is the near infrared false color composite (bands used being near infrared, red and green) (Figure 9).

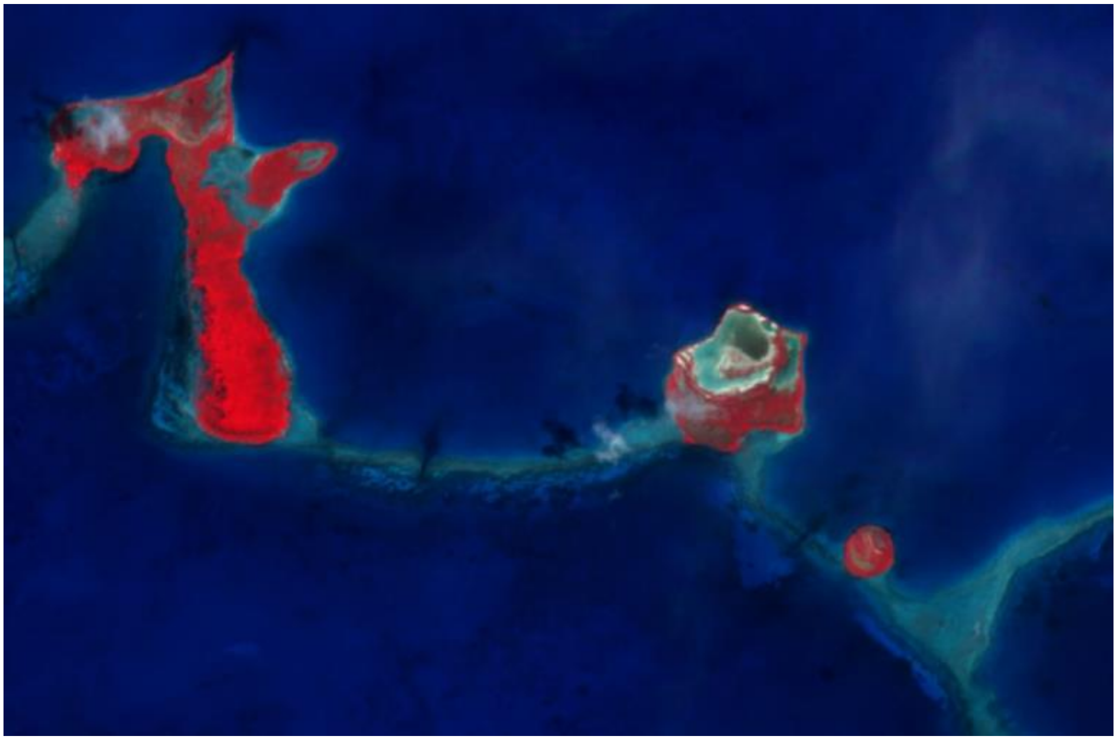

Figure 10. An example of a false color composite. The false color composite bands are organized as bands 8, 4, and 3 (near infra-red (NIR), red, and green allocated to the red, green, and blue color planes). This type of false color composite is widely used for studying vegetation distributions. For the purpose of this research, we use it to study mangrove species distribution in the Caribbean. This color composite shows the distinction between red (bright red) and black (dull red) mangroves within an island.

Discrimination of mangrove species occurs at the spectral level. We use Sentinel-2 satellite multispectral imagery for species discrimination. Sentinel-2 Multispectral Instrument (MSI) imagery offers the best resolution for data analysis of mangrove ecosystems across the Caribbean: 10 m by 10 m for the bands we used, compared to the 30 m by 30 m resolution of multispectral Landsat 7 and Landsat 8 imagery. Using Sentinel-2 allows resolution at a 10 m scale when using bands 8, 4 and 3 to build near infrared false color composites. Black mangroves have lower visible and NIR reflectance than red mangroves (Everett et al. 2008, Everett et al. 1989). Healthy red mangroves have higher chlorophyll content in their leaves, which allow them to reflect more near infrared wavelength sunlight than black mangroves. When assessing differences in vegetation, RGB = NIR, Red, Green (NRG) false color composites are predominantly used because the leaves of green vegetation reflect more NIR sunlight, which allows for the study of condition, type, and their changes in vegetated ecosystems. In order to differentiate between red and black mangrove areas, we used a NRG false color composite to distinguish red and black mangroves areas (Figure 10). Based on literature (Thomas et al. 2017, Giri et al. 2011), we verified that these are in fact red and black mangroves. From there, spectral plots were created based on areas of interest (AOI's).

The area of red mangroves within an island, can give us a clue as to how salinity moves throughout an island. Creating spectral plots, we can discriminate red mangrove areas using their spectral reflectance (Figure 11). A spectral plot indicates the mean surface reflectance of a given AOI within an image with respect to wavelength. Using each band (at different wavelengths) the spectral plot can indicate separation in reflection between black and red mangroves. Chlorophyll content greatly affects the reflectivity of both red and black mangroves. In a spectral plot, you can see the distinction between red and black mangroves most clearly in bands 6, 7, 8a, and 13. The range given by the spectral plot indicates the range of values used to distinguish red from black mangroves.

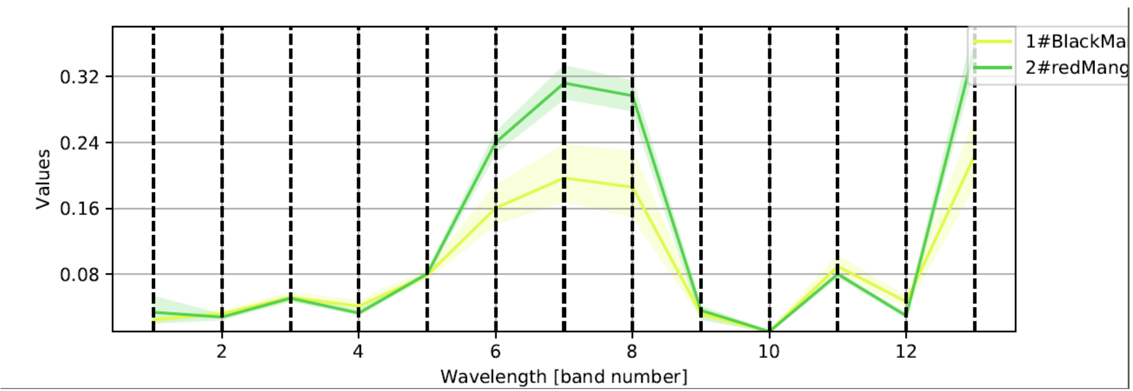

Figure 11. The spectral reflectance separation of red and black mangroves across the thirteen Sentinel-2 MSI bands. The greatest separation between red and black mangroves occurs in bands 7 and 8 (both NIR bands, with central wavelengths of 783 nm and 833 nm, respectively).

Band 6 (741 nm) also has a high separation with respect to mangrove type, which is why it is also used in vegetation separation (it is a vegetation "Red Edge" band). The purpose for using band 8 for mangrove separation is because it provides 10 m spatial resolution (while bands 6, 7, and 8a are all acquired at a nominal 20 m spatial resolution). and because other authors have used band 8 for mangrove ecosystems specifically (Everett et al. 2008, Everett et al. 1989). Band 8 (NIR band) is used to separate red and black mangroves given that it is one of the best separation bands for vegetation as well as the fact that the spectral plots indicate a large range between red and black mangroves (Thomas et al. 2017). We performed a spectral analysis of each island that confirms the existence of red and black mangroves. Spectral reflectance plots are created for each island since reflectivity can be affected not only by mangrove chlorophyll content, but also by soil moisture, water vapor and any atmospheric particles (aerosols).

3. Results

Despite the simplicity of the model, it quantitatively captures the relationship between net evaporation rates and mangrove islands vegetated area across the Caribbean (Figure 12). Model predictions, however, tend to underestimate mangrove vegetated areas observed in the field. This can be due to numerous factors that the model does not capture, such as other effects associated with mangrove degradation. Future work will explore additional factors to better understand the effect of net evaporation rates on mangrove ecosystems.

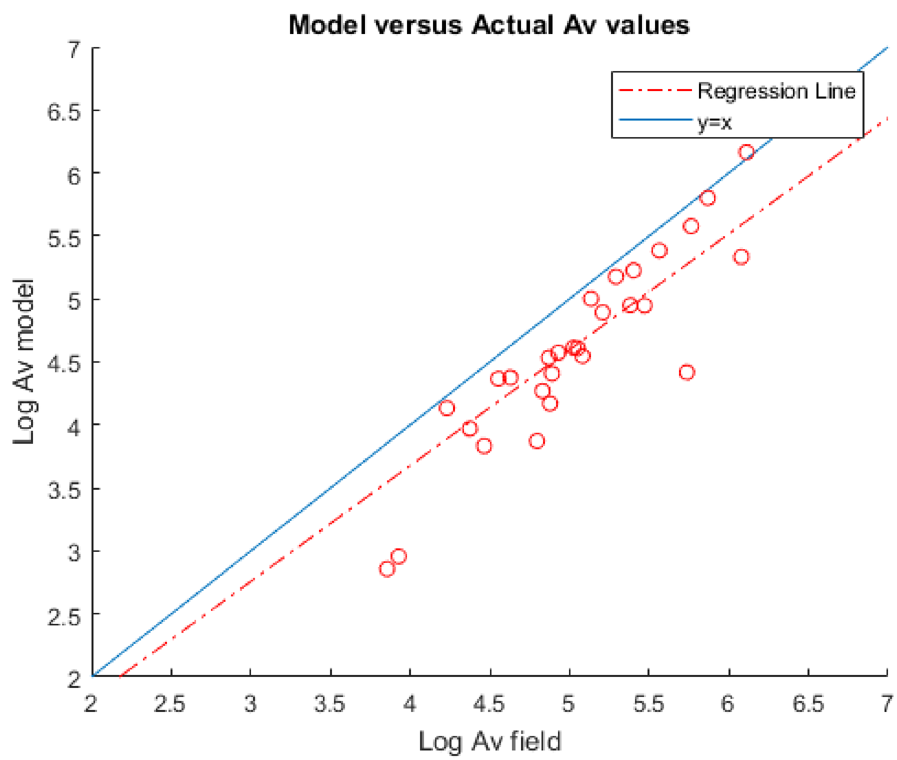

Figure 12. .Comparison between the model predictions and field observations, showing the strong agreement between them.

TABLE 1. PARAMETERS USED IN THE MODEL

Parameter Symbol	**Parameter Description**	**Range of Parameter Values Used**	**References**
k	Hydraulic Conductivity	10-130 m/yr	Rezanezhad et al. 2016
So	Ocean Salinity	35-40 ppt	Schmidt et al. 2004
Sc_B	Critical salinity concentration for black mangroves	100 ppt	Twilley et al. 1992, Cintron et al. 1978
$Enet$	Net evaporation	0-2 m/yr	
b	Conversion factor describing the salinity concentration over a characteristic depth	1 ppt/m	
Sc_R	The critical salinity of red mangroves	72 ppt	Cintron et al. 1978

4. Conclusions and Future work

As climate continues to warm, Caribbean mangrove islands will undergo changes in species zonation and forest degradation. The beneficial ecosystem services mangroves provide decrease as their vegetated area is reduced, partly due to increasing average positive net evaporation rates through time. Spatially, there is a trend where reduction in vegetated area can be seen in systems where high net evaporation rates occur. As they continue to decrease rapidly, these highly productive ecosystems are likely to become endangered. Our simple soil stressor balance model captures the effects of positive net evaporation on mangrove islands, as demonstrated by comparisons with observations. Changes in net evaporation clearly disrupt the soil stressor balance within an island, thus altering the vegetated area after the critical soil stressor concentration threshold is reached. Although this is a simple soil stressor balance model, it captures the effects of net evaporation rates on mangrove vegetation given the net evaporation rate, hydraulic conductivity, ocean salinity, and the critical salinity concentration threshold, allowing us to predict how mangrove vegetation will react, given specific net evaporation rates. With satellite multispectral remote sensing, we were able to distinguish red and black mangrove area using near infrared composite imagery: an important indicator of hydraulic conductivity within a mangrove island.

Future analysis will focus on exploring the likely roles of changes from the various environmental and biological drivers at different time scales on mangrove ecosystems. Environmental changes – i.e., changes in the temporal distributions of temperature, evaporation, salinity, and inundation, as well as competition – can affect mangrove vegetation by increases soil stressor concentrations within the ecosystem, causing mangrove degradation. This new research direction will leverage two sets of codes based on the number of bands available: one for Landsat 1 - 3 and another for Landsat 4, 5, 7 and 8 (Landsat 6 failed to reach orbit on launch in 1993). Additionally, I plan to extend the numerical model to account for medium- to long-term variations in different parameters, including the net evaporation rate and the ocean salinity. To calculate ocean salinity, I plan to use data from the NASA/Argentina space agency, (Comisión Nacional de Actividades Espaciales, CONAE) Aquarius/ SAC-D mission, which has a combined active/passive microwave (L-band) instrument that detects changes in ocean surface salinity. Salinity data per island will be used to study its effect on mangrove vegetation.

References

Alongi, D. M. (2008). Mangrove forests: resilience, protection from tsunamis, and responses to global climate change. *Estuarine, Coastal and Shelf Science*, *76*(1), 1-13.

Armenteros, M., Martin, I., Williams, J. P., Creagh, B., González-Sansón, G., & Capetillo, N. (2006). Spatial and temporal variations of meiofaunal communities from the western sector of the Gulf of Batabanó, Cuba. I. Mangrove systems. *Estuaries and coasts*, *29*(1), 124-132.

Ball, M. C. (1988). Salinity tolerance in the mangroves Aegiceras corniculatum and Avicennia marina. I. Water use in relation to growth, carbon partitioning, and salt balance. Functional Plant Biology, 15(3), 447-464.

Barbier, E. B. (2016). The protective service of mangrove ecosystems: A review of valuation methods. Marine pollution bulletin, 109(2), 676-681.

Boudreau, J., Caron, J., Elrick, D., Fortin, J., & Gallichand, J. (2009). Solute transport in sub-irrigated peat-based growing media. Canadian journal of soil science, 89(3), 301-313.

Cahoon, D. R., & Lynch, J. C. (1997). Vertical accretion and shallow subsidence in a mangrove forest of southwestern Florida, USA. Mangroves and Salt Marshes, 1(3), 173-186.

Chen, R., & Twilley, R. R. (1998). A gap dynamic model of mangrove forest development along gradients of soil salinity and nutrient resources. Journal of ecology, 86(1), 37-51.

Cintron, G., Lugo, A. E., Pool, D. J., & Morris, G. (1978). Mangroves of arid environments in Puerto Rico and adjacent islands. Biotropica, 110-121.

Giri, C., Ochieng, E., Tieszen, L. L., Zhu, Z., Singh, A., Loveland, T., ... & Duke, N. (2011). Status and distribution of mangrove forests of the world using earth observation satellite data. Global Ecology and Biogeography, 20(1), 154-159.

Granek, E. F., & Ruttenberg, B. I. (2007). Protective capacity of mangroves during tropical storms: a case study from 'Wilma'and 'Gamma'in Belize. Marine Ecology Progress Series, 343, 101-105.

Jimenez, J. A., Lugo, A. E., & Cintron, G. (1985). Tree mortality in mangrove forests. Biotropica, 177-185.

Krauss, K. W., Doyle, T. W., Doyle, T. J., Swarzenski, C. M., From, A. S., Day, R. H., & Conner, W. H. (2009). Water level observations in mangrove swamps during two hurricanes in Florida. Wetlands, 29(1), 142-149.

Lagerloef, G., Colomb, F. R., Le Vine, D., Wentz, F., Yueh, S., Ruf, C., ... & Feldman, G. (2008). The Aquarius/SAC-D mission: Designed to meet the salinity remote-sensing challenge. *Oceanography*, *21*(1), 68-81.

Lightbody, A. F., & Nepf, H. M. (2006). Prediction of velocity profiles and longitudinal dispersion in salt marsh vegetation. Limnology and oceanography, 51(1), 218-228.

Liu, Z., Ostrenga, D., Teng, W., & Kempler, S. (2012). Tropical Rainfall Measuring Mission (TRMM) precipitation data and services for research and applications. Bulletin of the American Meteorological Society, 93(9), 1317-1325.

Lovelock, C. E., Ball, M. C., Feller, I. C., Engelbrecht, B. M., & Ling Ewe, M. (2006). Variation in hydraulic conductivity of mangroves: influence of species, salinity, and nitrogen and phosphorus availability. *Physiologia Plantarum*, *127*(3), 457-464.

Lugo, A. E., & Snedaker, S. C. (1974). The ecology of mangroves. Annual review of ecology and systematics, 5(1), 39-64.

Padrón, C. M., Llorente, S. O., & Menendez, L. (1993). Mangroves of Cuba. *Conservation and Sustainable Utilization of Mangrove Forests in Latin America and Africa Regions, Part I-Latin America"(LD Lacerda, ed)*, 147-154.

Parida, A., Das, A. B., & Das, P. (2002). NaCl stress causes changes in photosynthetic pigments, proteins, and other metabolic components in the leaves of a true mangrove, Bruguiera parviflora, in hydroponic cultures. Journal of Plant Biology, 45(1), 28-36.

Phang, V. X., Chou, L. M., & Friess, D. A. (2015). Ecosystem carbon stocks across a tropical intertidal habitat mosaic of mangrove forest, seagrass meadow, mudflat and sandbar. *Earth Surface Processes and Landforms*, *40*(10), 1387-1400.

Rezanezhad, F., Price, J. S., Quinton, W. L., Lennartz, B., Milojevic, T., & Van Cappellen, P. (2016). Structure of peat soils and implications for water storage, flow and solute transport: A review update for geochemists. Chemical Geology, 429, 75-84.

Schmidt, M. W., Spero, H. J., & Lea, D. W. (2004). Links between salinity variation in the Caribbean and North Atlantic thermohaline circulation. *Nature*, *428*(6979), 160.

Tavares, R. (2001). Estudio sobre Biodiversidad de Tiburones en el Parque Nacional Archipiélago de los Roques (Segunda Etapa). Oficina Nacional de Diversidad Biológica/MARN, Caracas. Inf. Téc./2001-0074.

Thomas, N., Lucas, R., Bunting, P., Hardy, A., Rosenqvist, A., & Simard, M. (2017). Distribution and drivers of global mangrove forest change, 1996–2010. *PloS one*, *12*(6), e0179302.

Twilley, R. R., Chen, R. H., & Hargis, T. (1992). Carbon sinks in mangroves and their implications to carbon budget of tropical coastal ecosystems. *Water, Air, and Soil Pollution*, *64*(1-2), 265-288.

Urish, D. W., Wright, R. M., Feller, I. C., & Rodriguez, W. (2009). Dynamic Hydrology of a Mangrove Island: Twin Cays, BelizeEM8. Smithsonian Contributions to the Marine Sciences, (38).

Yu, L., Jin, X., & Weller, R. A. (2008). Multidecade Global Flux Datasets from the Objectively Analyzed Air-sea Fluxes (OAFlux) Project: Latent and sensible heat fluxes, ocean evaporation, and related surface meteorological variables. OAFlux Project Technical Report. OA-2008-01, 64pp.

Appendix

A1. Methods for TRMM data extraction

The Tropical Rain Monitoring Mission provides precipitation rates in tropical and subtropical regions in hourly, daily and monthly datasets. The datasets are available in NetCDF data files which is a common format for downloading climate data. To build the precipitation map used in calculating the values for the net evaporation map, we download monthly datasets ranging from 1997- 2016 (all available monthly datasets from the TRMM satellite platform). Each pixel within the imagery contains a specific value for precipitation located within that coordinate where the precipitation units in centimeters per month. To build an precipitation map encompassing the average precipitation value over the span of 16 years, we first needed to build yearly precipitation maps. Each yearly precipitation map encompasses 12 monthly precipitation maps averaged into one map showing the average precipitation for a specific given year. This process is then repeated for the rest of the years within the dataset. After completing 18 yearly precipitation maps, we then build 1 precipitation map showing the averaged precipitation values over an 18 year timespan.

TRMM Data Links:

https://mirador.gsfc.nasa.gov/cgi-bin/mirador/presentNavigation.pl?tree=project&dataset=3B43:%20Monthly%200.25%20x%200.25%20degree%20merged%20TRMM%20and%20other%20sources%20estimates&project=TRMM&dataGroup=Gridded&version=7&CGISESSID=e3d209d18c67914758b21911d4fc391f

https://disc.gsfc.nasa.gov/datasets/TRMM_3B43_V7/summary

A2. Methods to extract evaporation rates

The Woods Hole Oceanographic Institute provides evaporation datasets ranging from 1956 to present. The datasets are available in NetCDF format which is a common format used for storing climate data and allows for similar processing to the TRMM datasets. The evaporation datasets are available in yearly packages where each pixel within an image represents the average evaporation rate for a given year within that given space. Since it is available in yearly datasets, we use datasets from 1997-2016 to build an average evaporation map. We specifically use these years to overlap with the years available in TRMM datasets. Using the 18 years of data from the Woods Hole OAFLUX project, we build an evaporation map that describes the average evaporation across the Caribbean within the 18-year timespan. From this map, we then Georefence the image to overlay the Caribbean, and from there we build a net evaporation map.

WHOI Data Links:
http://oaflux.whoi.edu/evap.html
ftp://ftp.whoi.edu/pub/science/oaflux/data_v3/monthly/evaporation/

The net evaporation map is built using an averaged 18-year span of data from Woods Hole's evaporation data and TRMM precipitation data. From the model, we use a simple equation to calculate the net evaporation across the Caribbean where $net\ evaporation = evaporation\ (map) - precipitation\ (map)$.

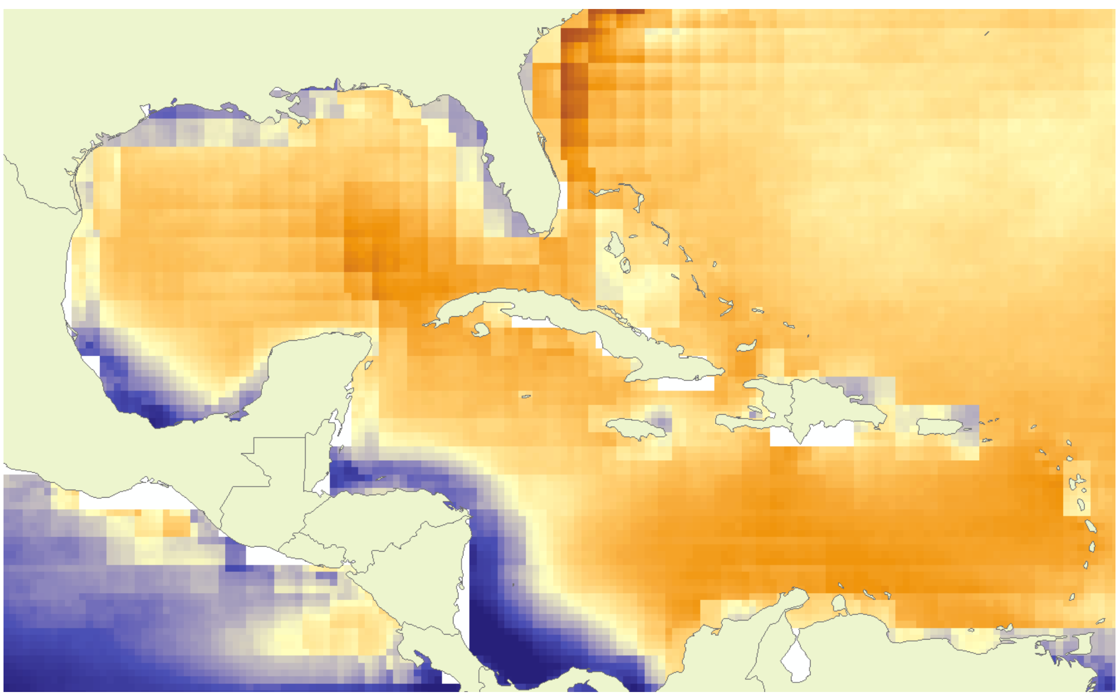

From the map (shown above) we can then determine that the Caribbean lies in a predominantly positive net evaporation zones. Thus, we can then begin to hypothesize which mangrove islands will be most affected from increased soil stressor concentrations derived from high net evaporation rates.

A3. Mangrove island exploration

Mangrove islands are explored using Google Earth Inc. imagery and validating whether it is in fact a mangrove islands using Global Forest Watch. Global Forest Watch has a 99% accuracy rate in whether determining if an area is, in fact, a mangrove island. In this section of the appendix, we explore the different islands across the Caribbean which we gathered information on, for the purpose of this study.

Global Mangrove Watch: https://www.globalforestwatch.org/

Examples of island locations:

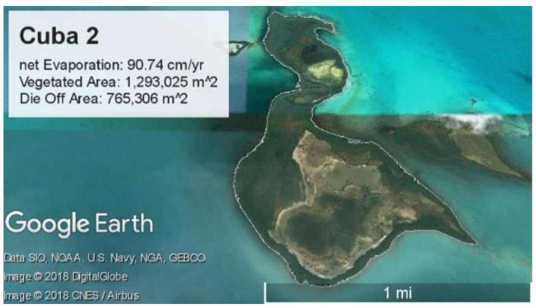

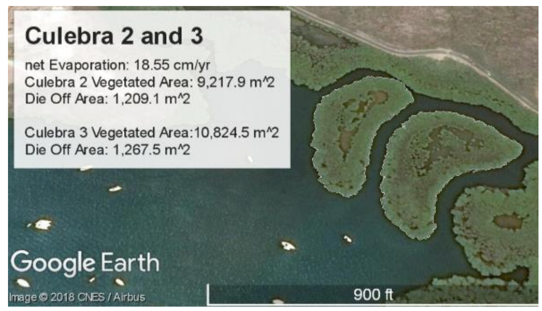

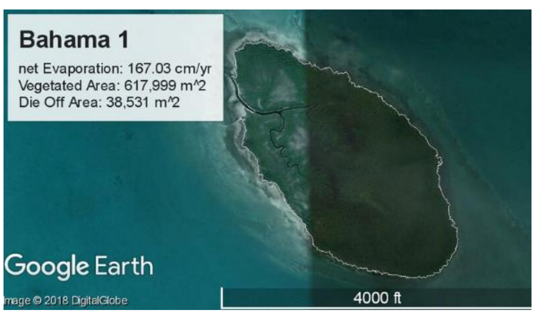

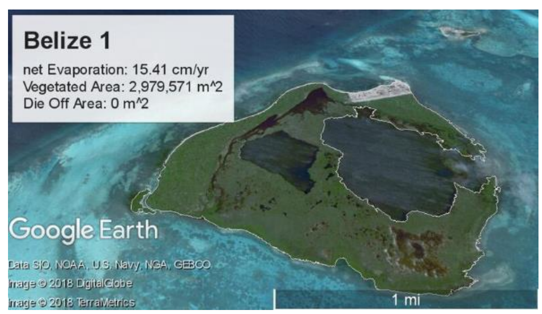

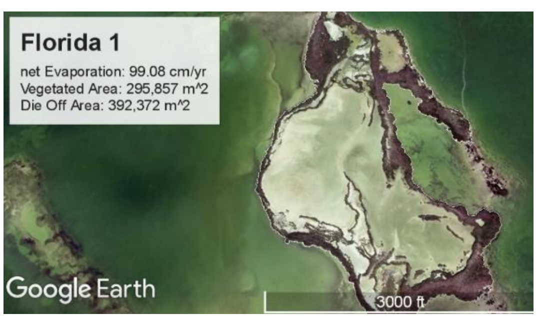

Table: Mangrove Island Database

Island Name	Coordinates	Area (m^2)	Vegetated Area (m^2)	Die Off Area (m^2)	Net evaporation (cm/yr)	Red Mangrove Area (m^2)	Black Mangrove Area (m^2)	% red mangrove	So (ppt)	k (hydraulic conductivity) m^2/yr
PuertoRico1	17°58'12.20"N 66°59'57.56"W	13661	8487	5174	84.51	4800	3687	35.13652002	35	17.45773799
PuertoRico2	17°58'14.66"N 66°59'52.02"W	9045	7174	1871	84.57	3598	3576	39.77888336	35	13.09532019
PuertoRico5	17°57'31.46"N 67° 5'32.86"W	20878	17014	3864	64.05	13582	3432	65.05412396	35	37.43876313
PuertoRico7	17°58'5.89"N 67° 0'5.71"W	32807	23700	9107	64.05	11454	12246	34.9132807	35	31.57293424
PuertoRico3	17°58'58.86"N 66°44'15.30"W	87153	67701	19452	85.59	25870	41831	29.68343029	35	95.29236099
PuertoRico6	17°58'27.77"N 66°44'49.82"W	86429	85012	1417	85.59	103476	-18464	119.7237038	35	381.1547099
Belize1	17°26'51.10"N 87°30'15.33"W	2979571	2979571	0	14.26	2114951	864620	70.98172858	35	1297.951509
Mexico1	21°25'31.16"N 86°52'44.15"W	1,299,823	1197621	102,202	50.72	257810	939811	19.83423897	35	562.752763
Florida1	25° 3'21.29"N 80°41'45.93"W	688229	295857	392372	72.42	89658	206199	13.02734991	35	279.4384731
Florida2	25° 2'55.51"N 80°42'11.58"W	51434	29122	22312	72.42	7860	21262	15.28172026	35	24.49738337
Florida3	25° 3'32.97"N 80°35'10.20"W	387786	241064	146722	72.42	70138	170926	18.08677982	35	218.6001876
Florida4	25° 9'36.62"N 80°33'10.14"W	140474	112319	28155	72.42	48675	63644	34.65054031	35	151.7061241
Florida5	25° 2'3.48"N 80°38'50.56"W	135257	77645	57612	72.42	38657	38988	28.58040619	35	120.4828688
Florida6	25° 1'33.10"N 80°38'54.17"W	37028	35737	1291	72.42	18341	17396	49.532786	35	57.16367791
Bahamas1	26°54'58.97"N 78°36'48.44"W	579468	579468	0	104.43	297905	281563	51.41008649	35	1338.880149
Venezuela1	11°49'36.72"N 66°35'40.44"W	177239	161227	16012	149.04	61597	99630	34.75363774	35	395.0945464
Venezuela2	11°50'32.33"N 66°36'4.58"W	421560	366635	54925	149.04	230642	135993	54.71154759	35	1479.38043
Cuba2	22° 8'18.38"N 81°54'0.52"W	2058331	1293025	765306	72.34	1148204	144821	55.78325352	35	3574.671947
Cuba3	22°30'15.50"N 82°20'16.28"W	146487	42603	103884	62.25	18698	23905	12.7642726	35	50.09255035
CrabKey	24°59'17.87"N 80°40'10.30"W	138085	136350	1735	140.67	78921	57429	57.15392693	35	477.785207
CrabKey2	24°59'30.15"N 80°39'38.58"W	571651	544291	27360	140.67	20626	523665	3.608145529	35	124.8691436
ButtonwoodKey	25° 4'1.35"N 80°43'54.54"W	642839	252404	390435	72.42	132522	119882	20.61511514	35	413.0333637
ButtonwoodKey2	25° 5'4.92"N 80°43'27.95"W	99877	75396	24481	72.42	11630	63766	11.64432252	35	36.24740059
CraneKey	25° 0'2.13"N 80°37'29.34"W	121746	120650	1096	106.54	27789	92861	22.82539057	35	127.4160811
SidKey	25° 1'29.79"N 80°47'17.81"W	229955	106110	123845	55.43	32381	73729	14.08145072	35	77.24560294
TopsyKey	25° 2'36.81"N 80°46'35.13"W	110299	74044	36255	55.43	26900	47144	24.38825375	35	64.17055431
ShellKey	24°55'23.54"N 80°39'57.07"W	2058331	737302	1321029	140.67	538999	198303	26.18621592	35	3263.082688
BarnesKey	24°56'19.43"N 80°47'7.71"W	291211	195762	95449	100.78	126223	69539	43.34417313	35	547.4588544
UpperArsnickerKey	24°55'55.37"N 80°49'39.08"W	62553	62553	0	100.78	5875	56678	9.392035554	35	25.48125753

A4. Derivation of Vegetated Area equation

Since we are treating these islands as circular islands, we have to take into account the area of a circular ($A = \pi R^2$). The area for the die off (A_d) would then be $A_d = \pi X_c^2$. The area from vegetation comes out to be $A_v = A - A_d$: which is also the same equation as $A_v = \pi R^2 - \pi X_c^2$. This is the equation used to calculate vegetated area when using Google Earth imagery. In order to achieve a curve which explains how islands respond to different net evaporation values, original second order differential equation is solved using x_c for x while having the equation equal Sc (critical salinity concentration). We also multiply this equation by pi since we are assuming that these islands are circular:

$$Sc = -\alpha x_c^2 + So + \alpha R^2$$

$$\pi(Sc) = \pi(-\alpha x_c^2 + So + \alpha R^2)$$

$$\frac{1}{\alpha}(\pi Sc) = (-\pi\alpha x_c^2 + \pi So + \pi\alpha R^2)\frac{1}{\alpha}$$

$$\frac{1}{\alpha}\pi Sc = -\pi x_c^2 + \frac{1}{\alpha}\pi So + \pi R^2$$

$$\frac{1}{\alpha}\pi Sc - \frac{1}{\alpha}\pi So = -\pi x_c^2 + \pi R^2$$

Since $Av = -\pi x_c^2 + \pi R^2$, the vegetated area equation gets rearranged to be $Av = \frac{Sc-So}{\alpha}\pi$.

A5. Codes in Matlab software

(Multiple vegetated curves with field observations)

```
%% input parameters for PDE
D=5; %Diffusivity m^2/yr
Da=50;
Db=90;
Dc=130; %Different diffusion values
Sc=82; %Salinity concentration at tree death. (Cintron et al. 1978)
(ppt)
So=35;% (ppt ocean salinity average)
Sos=45; %Second Ocean salinity value
ETnet=linspace(0.01,2,1001); %m/yr
b=1 %conversion factor


% for i=1:n
Av=((Sc-So)*2*pi*D)./(ETnet)*(35*b);
Ava=((Sc-Sos)*2*pi*D)./(ETnet)*(35*b);

Avb=((Sc-So)*2*pi*Da)./(ETnet)*(35*b);
Avc=((Sc-Sos)*2*pi*Da)./(ETnet)*(35*b);

Avd=((Sc-So)*2*pi*Db)./(ETnet)*(35*b);
Ave=((Sc-Sos)*2*pi*Db)./(ETnet)*(35*b);

Avf=((Sc-So)*2*pi*Dc)./(ETnet)*(35*b);
Avg=((Sc-Sos)*2*pi*Dc)./(ETnet)*(35*b);
% end
px= [0.8451 0.8457 .6405 .6405 .8559 .8559 .1426 .5072 .7242 .7242
.7242 .7242 .7242 .7242 1.0443 1.4904 1.4904 .7234 .6225 1.4067 1.4067
.7242 .7242 1.0654 .5543 .5543 1.4067 1.0078 1.0078];
py= [8487 7174 17014 23700 67701 85012 2979571 1197621 296857 29122
241064 112319 77645 35737 579468 161227 366635 1293025 42603 136350
544291 252404 75396 120650 106110 74044 737302 195762 62553];

figure (1)
plot(ETnet,Av*10^-6,'b',ETnet,Ava*10^-6,'b--',ETnet,Avb*10^-
6,'g',ETnet,Avc*10^-6,'g--',ETnet,Avd*10^-6,'r',ETnet,Ave*10^-6,'r--
',ETnet,Avf*10^-6,'k',ETnet,Avg*10^-6,'k--',px,py*10^-6,'ko')

%loglog(ETnet,Av,'r')
figure(1)
hold on
 xlabel('Net Evaporation (m/yr)')
 ylabel('Av (km^2)')
 title('Vegetated Area')
 legend('k=10 m/yr So=35 ppt','k=10 m/yr So=40 ppt','k=50 m/yr So=35
ppt','k=50 m/yr So=40 ppt','k=90 m/yr So=35 ppt','k=90 m/yr So=40
ppt','k=130 m/yr So=35 ppt','k=130 m/yr So=40 ppt')
legend boxoff
 axis([0 1.8 0 3])
```

(Log Av model versus log Av field)

```
clear all;
x=0:0.1:7;

n=length(x);
y=zeros(1,n);
ya=zeros(1,n);

y=0.9195*x;
ya=x;

px= [3.928754202    3.855761372 4.230806428 4.374748346 4.830595084
4.929480234 6.474153739 6.078319403 5.471081849 4.464221198 5.382132359
5.050453228 4.890113494 4.553118092 5.763029458 5.207437773 5.564233922
6.111606922 4.629440182 5.134655142 5.735831153 5.402096233 4.877348306
5.081527326 5.025756315 4.869489872 5.867645412 5.291728393
4.796248143]
py= [2.956376128    2.857479193 4.133279912 3.970714937 4.269793044
4.573821191 6.427138124 5.334339946 4.946804784 3.833222944 4.949849512
4.609602196 4.407243412 4.367319145 5.577973926 4.893455695 5.384114719
6.163915189 4.375691289 5.001088713 4.418311147 5.226184115 4.169475849
4.547769053 4.614186391 4.533648414 5.801995809 5.17659811
3.872904005]

hold on
plot(x,y,'-.r',x,ya,'b',px,py,'ro')
xlabel('Log (Vegetated Area) field')
ylabel('Log (Vegetated Area) model')
title('Model versus Actual Vegetated Area values')
legend('Regression Line','y=x')
legend boxoff

axis([2 7 2 7])
```

Hydraulic conductivity regime plot:

```
% clc
% clear all
% close all

Enet=linspace(0.14,2,1000);
D=linspace(0,3000,1000);
So=35;
b=1;
Sc=72;

ne=length(Enet);
nd=length(D);
Av = zeros(ne,nd);
Av_km = zeros(ne,nd);

for i=1:nd
    for j=1:ne
```

```
        Av(i,j)=((Sc-So)*(2*pi*D(i)/(Enet(j)*b)));
        Av_km(i,j)=Av(i,j)/(1e6);
    end
end
px= [0.8451 0.8457 .6405 .6405 .8559 .8559 .1426 .5072 .7242 .7242
.7242 .7242 .7242 .7242 .0328 1.0443 .038 1.4904 1.4904 .7234 .6225
1.4067 1.4067 .7242 .7242 1.0654 .5543 .5543 1.4067 1.0078 1.0078];
py= [8487 7174 17014 23700 67701 85012 2979571 1197621 296857 29122
241064 112319 77645 35737 116179 579468 677416 161227 366635 1293025
42603 136350 544291 252404 75396 120650 106110 74044 737302 195762
62553];

figure (1)
pcolor(Enet,D,Av_km)
%contour(Enet,D,Av)
axis([0.14 1.6 0 3000]);
shading flat
hold on
```

Red Mangrove regime plot:

```
clc
clear all
close all

Enet=linspace(0.1,2,100);
Ar=linspace(1,2200000,100);
So=35;
b=1;
Sc=72;

ne=length(Enet);
na=length(Ar);

D = zeros(ne,na);

for i=1:na
    for j=1:ne
        D(i,j)=(Enet(j)*Ar(i))/(2*pi*(Sc-So));
    end
end
%px= [0.8451 0.8457 .6405 .6405 .8559 .1426 .5072 .7242 .7242 .7242
.7242 .7242 .7242 1.4904 1.4904 .7234];
%py= [712 567 10700 7359 14652 2104951 169998 69648 5362 70138 32041
20107 18341 61597 190642 1148204];

figure(1)
pcolor(Enet,Ar*10^-6,D)
hold on
%plot(px,py)%'go')
shading flat
xlabel('Net Evaporation (m/yr)')
ylabel('Red mangrove area km^2')
title('Hydraulic Conductivity')
hold on
contour(Enet,Ar*10^-6,D,'k')
```